



## Reaction model for kinetic of cobalt dissolution in carbonate/bicarbonate media

J.A. Calderón<sup>a,1</sup>, O.E. Barcia<sup>b</sup>, O.R. Mattos<sup>b,\*</sup>

<sup>a</sup> Corrosion and Protection Group, University of Antioquia, Calle 62 No. 52-59, P.O. Box 1226, Medellín, Colombia

<sup>b</sup> Laboratório de Corrosão Professor Manoel de Castro, PEMM/COPPE/UF RJ, Cx Postal 68.505, CEP 21945-97, Rio de Janeiro, RJ, Brazil

### ARTICLE INFO

#### Article history:

Received 10 April 2008

Accepted 22 April 2008

Available online 29 April 2008

#### Keywords:

A. Cobalt

A. Carbonate/bicarbonate

B. EIS

C. Cobalt electrodisolution

C. Reaction model

### ABSTRACT

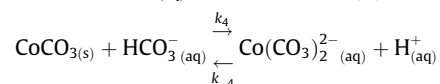
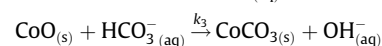
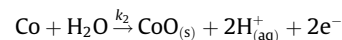
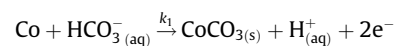
Cobalt dissolution in a carbonate/bicarbonate media was studied in order to elucidate the kinetic of the metal corrosion processes. Steady-state polarization and electrochemical impedance measurements were carried out during the active metal dissolution at different electrode rotation speeds. A reaction mechanism is presented in order to explain the metal dissolution: cobalt electrodisolution starts with the formation of intermediate  $(\text{CoHCO}_3)_{\text{ads}}$  on the electrode surface, followed by the simultaneous formation of a  $\text{Co}(\text{CO}_3)_2^{2-}$  complex and the formation of a CoO film. Mass transport is characterised by diffusion of the  $\text{Co}(\text{CO}_3)_2^{2-}$  complex away from the electrode. The reaction model was validated by an accurate simulation of the experimental steady-state polarisation and impedance measurements.

© 2008 Elsevier Ltd. All rights reserved.

### 1. Introduction

Cobalt industrial applications have increased over the last 20 years for biomedical alloys, magnetic films, high temperature corrosion-resistant alloys, among other uses. This demand has created the need to study cobalt corrosion and its behaviour in different environments [1–4]. In strong and weak alkaline media cobalt shows an active–passive behaviour, with distinct dissolution and passivation steps [5–10].

Davies and Burstein [11,12] studied cobalt behaviour in a carbonate/bicarbonate media using potentiodynamic polarisation, spectroscopy techniques and thermodynamic data. A series of reactions that govern the first step of cobalt dissolution and passivation were proposed:



The most important features in the reaction scheme suggested by Davies and Burstein are: (i) CoO film formation during the active cobalt dissolution and (ii) the existence of a cobalt carbonate complex, corroborated by chemical analysis [11]. The  $\text{Co}(\text{CO}_3)_2^{2-}$  complex ion

diffusion from the cobalt surface to the bulk solution can explain the mass transport control observed by the authors in the cobalt dissolution in this media. According to Davies and Burstein the mass transport control in the active dissolution of cobalt follows a linear relationship between the current and the square root of the rotation speed ( $I$  versus  $\Omega^{1/2}$ ), Levich type equation. In a previous work [13] we show that the mass transport involved in the cobalt active dissolution in a carbonate/bicarbonate media for different anodic potentials and different solution concentrations following a non linear behaviour for  $I$  versus  $\omega^{1/2}$  and for  $I^{-1}$  versus  $\omega^{-1/2}$ . The relationship between the anodic current and the rotation speed is not a classical Levich law and was analysed using the expression:

$$I_t = I_0 + \frac{1}{I_k^{-1} + A^{-1}\Omega^{-1/2}} \quad (1)$$

In this equation, the total current ( $I_t$ ) is composed of two partial processes, a non-diffusion current ( $I_0$ ) and the current given by the terms of the classical Koutecky-Levich expression ( $I_k$ ) and ( $A$ ). We obtained a very good fitting between experimental and calculated currents using Eq. (1) [13].

According to Davies and Burstein, the first cobalt passivation step in a carbonate/bicarbonate media occurs by the CoO film formation on the metal surface. Gervasi et al. [14–16] proposed a reaction scheme similar to the scheme already proposed by Davies and Burstein, but suggested that cobalt passivation occurs by the  $\text{Co}_3\text{O}_4$  film formation on cobalt, because the CoO film is reactive to  $\text{HCO}_3^-$  ion and does not protect the metal. In previous work, using in situ and ex situ Raman spectroscopy during anodic cobalt potentiostatic polarisation in a carbonate/bicarbonate media, we showed that a CoO film on the electrode surface is formed during

\* Corresponding author. Tel.: +55 21 25628550; fax: +55 21 22901544.

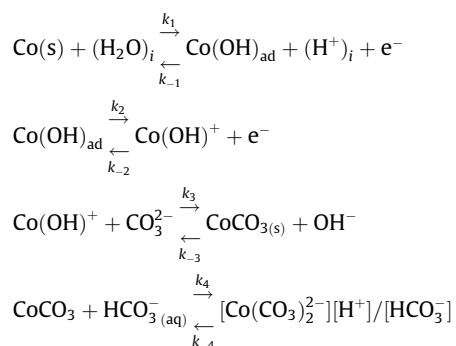
E-mail address: [omattos@metalmat.ufri.br](mailto:omattos@metalmat.ufri.br) (O.R. Mattos).

<sup>1</sup> Tel.: +57 4 2196617; fax: +57 4 2196565.

the active dissolution of the metal at low anodic potentials. Cobalt passivation occurs by a slow transformation of the CoO oxide into a Co<sub>3</sub>O<sub>4</sub> passive film [13].

Danick Gallant et al. [17,18] studied the cobalt behaviour in carbonate/bicarbonate solutions with different pH values and in presence of halide ions. Using a numerical deconvolution of the potentiodynamic curves, the authors found that the first and the second dissolution–passivation steps are heavily influenced by the solution pH [18]. Meanwhile, Real [19] studied cobalt electro-dissolution in a carbonate/bicarbonate media by electrochemical impedance. The impedance showed two capacitive loops in the first region of the active cobalt dissolution. The first loop at high frequencies was associated to the double layer capacitance and surfaces inhomogeneities. The second capacitive loop was associated with diffusion impedance, classical Levich law, related to the diffusion of the HCO<sub>3</sub><sup>-</sup> ion [19].

Recently Real et al. [20] proposed a reaction model for cobalt dissolution in a carbonate–bicarbonate media, where cobalt dissolves forming a Co(OH)<sub>ad</sub> intermediate-adsorbed species and this species participate at some equilibrium reactions with other adsorbed species as Co(OH)<sup>+</sup> and CoCO<sub>3</sub>, at the surface-solution interface:



It is interesting to emphasize that the model shown above has three adsorbed species to explain only one faradaic process coupled with mass transport. Moreover, the existence of CoO at the electrode surface, well confirmed by the literature [11–13], is not considered in the model.

The aim of this paper is to study the anodic behaviour of cobalt in a carbonate–bicarbonate media, by steady-state polarization and electrochemical impedance measurements (EIS) during the active metal dissolution at different electrode rotation speeds. The reaction model proposed in this work considers the existence of two intermediate species adsorbed on the metal surface and another complex species that diffuses away from the electrode. The reaction model was validated by a simulation of the experimental results using the same set of kinetic parameters for the polarisation and impedance data.

## 2. Experimental

For the electrochemical experiments a classical three-electrode cell was used. A 5 mm diameter cobalt cylindrical bar (Johnson Matthey Chemicals Ltd.) embedded in a epoxy resin that was used as the rotating disc electrode (RDE), with 0.2 cm<sup>2</sup> of exposed area. A saturated sulphate electrode (SSE) was used as a reference and the counter electrode was a large area platinum grid. All potential values in this paper are given versus the saturated sulphate electrode (SSE). The electrolyte consisted of 0.75 M KHCO<sub>3</sub> + 0.05 M K<sub>2</sub>CO<sub>3</sub>, the pH was constant at 8.9. The solutions were prepared from analytical grade chemicals and double distilled water, before using water it was previously boiled to remove dissolved CO<sub>2</sub>. During the measurements, electrolytes were de-aerated by purging

with purified nitrogen. Polarisation curves were carried out on the first active dissolution region of the metal, from the open-circuit potential (OCP) up to the current potential peak, just before metal passivation. The rotation speed of the working electrode was varied from 100 to 900 rpm. Electrochemical impedance measurements were made under potential control with a perturbation between 5–15 mV and frequencies scan from 40 kHz to 10<sup>-3</sup> Hz. Electrochemical measurements were made using an Autolab PGSTAT 30. A detailed description of the experimental setup and procedure can be found in a previous paper [13].

## 3. Results

### 3.1. Potentiostatic polarisation

Current–voltage curves were plotted at various rotation speeds of the cobalt disk electrode. Fig. 1 shows the polarisation curves for cobalt disk in 0.75 M KHCO<sub>3</sub> + 0.05 M K<sub>2</sub>CO<sub>3</sub> solution. As it was evidenced in a previous study [13] there is a complex coupling between mass transport and kinetic of the anodic process in the active dissolution region. Two different slopes at low and at high anodic potentials were also observed. This is consistent with the experimental polarisation measurements reported in the literature [11–13,17–20]. The presence of two slopes in the steady-state polarisation curves suggests that two different electrochemical paths are likely to be taking place during the anodic dissolution of cobalt. Fig. 2 shows the variation of the current density versus the square root of the rotation speed of the cobalt electrode for different potentials in 0.75 M KHCO<sub>3</sub> + 0.05 M K<sub>2</sub>CO<sub>3</sub> solution. Fig. 2 presents a non-linear behaviour between *I* versus Ω<sup>1/2</sup> and between *I*<sup>-1</sup> versus Ω<sup>-1/2</sup>. These curves are confirming a very complex mass transport process that can not be explained by the classical Levich equation as tried in [20]. These results were well fitted by the Eq. (1) for different anodic potentials in the active dissolution region of cobalt and for different solution concentrations, Fig. 3.

### 3.2. Electrochemical impedance

Fig. 4 shows the impedance plots for cobalt in a rotating disk electrode in 0.75 M KHCO<sub>3</sub> + 0.05 M K<sub>2</sub>CO<sub>3</sub> solution. The impedance measurements were made at different potentials in the active dissolution region and for different rotation speeds. The impedance plots consist of two capacitive loops in all experimental conditions. Similar impedance plots were obtained by Real for cobalt in car-

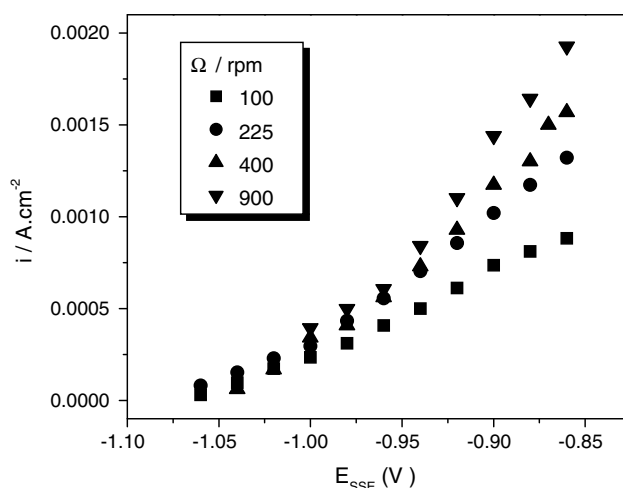
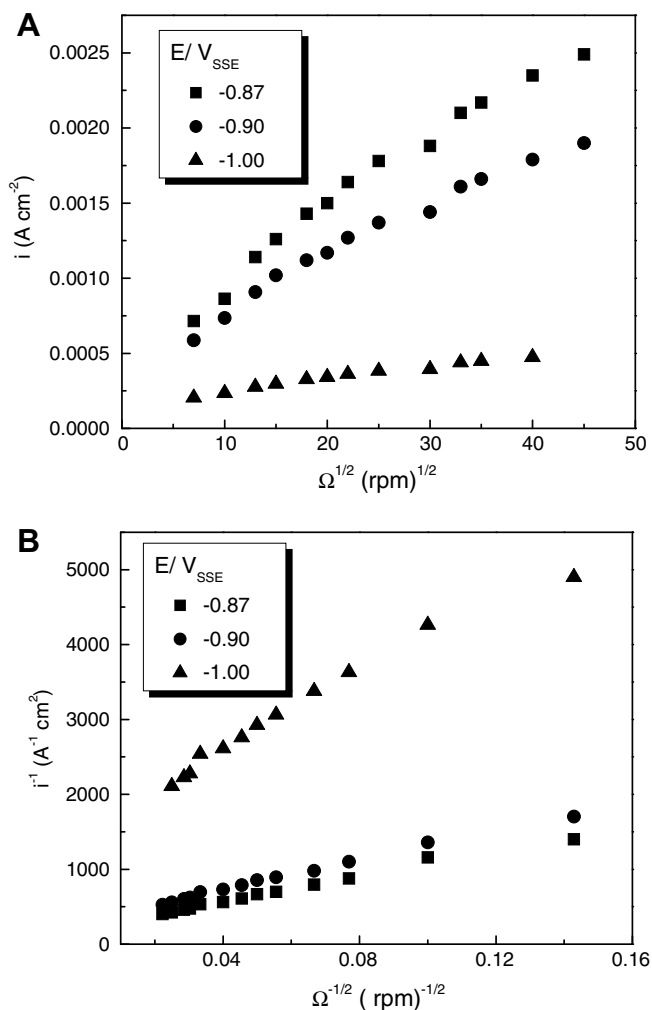


Fig. 1. Steady-state polarisation curves of cobalt in the active dissolution region in 0.75 M KHCO<sub>3</sub> + 0.05 M K<sub>2</sub>CO<sub>3</sub> solution and different rotation speeds.



**Fig. 2.** Anodic current versus rotation speed plots for cobalt dissolution in 0.75 M KHCO<sub>3</sub> + 0.05 M K<sub>2</sub>CO<sub>3</sub> solution at different anodic potentials. (A)  $I$  versus  $\Omega^{1/2}$  relationship. (B)  $I^{-1}$  versus  $\Omega^{-1/2}$  relationship.

bonate/bicarbonate media with different solution concentrations and pH values [19,20]. Near of the open-circuit potential the two loops are lightly coupled and as the anodic polarisation increases the loops become more separated and pronounced. These results indicate that anodic polarisation stimulates the formation and growth of the adsorbed specie on the cobalt surface. Fig. 4, also shows that the impedance values at limit of zero frequency decrease with the increase of the rotation speed. Additionally, at high anodic potentials the characteristic frequency of the second capacitive loop increases lightly with the increase of the rotation speed. These results show that the diffusion process is coupled with formation of adsorbed species representing the capacitive loop observed at low frequencies.

### 3.3. Surface behaviour

A black and non adherent film was formed on the cobalt surface after anodic polarisation of the rotating disk electrode in 0.75 M KHCO<sub>3</sub> + 0.05 M K<sub>2</sub>CO<sub>3</sub> solution. The increase in the anodic potential stimulated the formation and growth of the film. An extensive characterisation of the formed film by in situ and ex situ Raman spectroscopy was made [13]. The formed film in this first active dissolution region is composed by CoO oxide in accordance with the reports of others authors [11,12,14–16]; however the existence

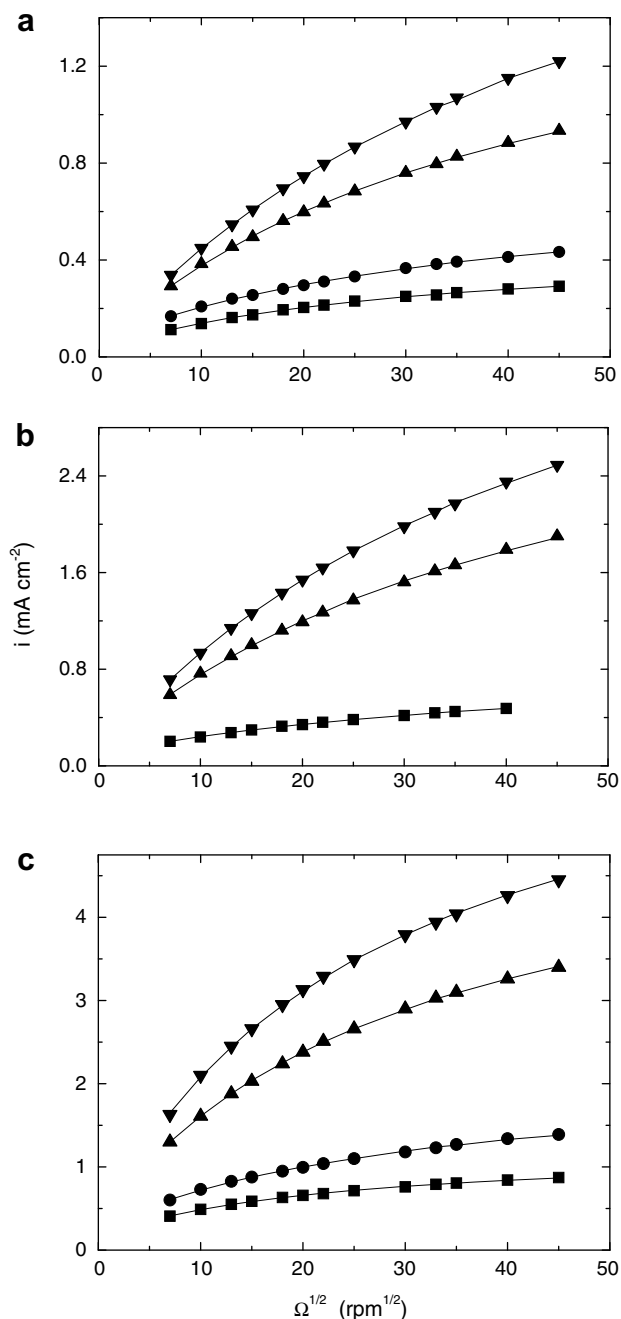


**Fig. 3.** Variation of anodic current density versus square root of the rotation speed in different carbonate/bicarbonate solutions and anodic potentials, pH = 8.9. (a) 0.375 M KHCO<sub>3</sub> + 0.025 M K<sub>2</sub>CO<sub>3</sub>, (b) 0.75 M KHCO<sub>3</sub> + 0.05 M K<sub>2</sub>CO<sub>3</sub>, (c) 1.5 M KHCO<sub>3</sub> + 0.1 M K<sub>2</sub>CO<sub>3</sub>. (■) -1.0 V, (●) -0.97 V, (▲) -0.90 V, (▼) -0.87 V, and (–) fitting using Eq. (1).

of CoCO<sub>3</sub> was not confirmed. Furthermore, the formation of the Co<sub>3</sub>O<sub>4</sub> oxide was observed only in the passive region.

## 4. Discussion

### 4.1. Construction of the reaction model

In a previous paper [13] we proposed a reaction model as a first approximation to explain the kinetic model of cobalt anodic dissolution in a carbonate/bicarbonate media, taking into account steady-state measurements and surface characterisation at different

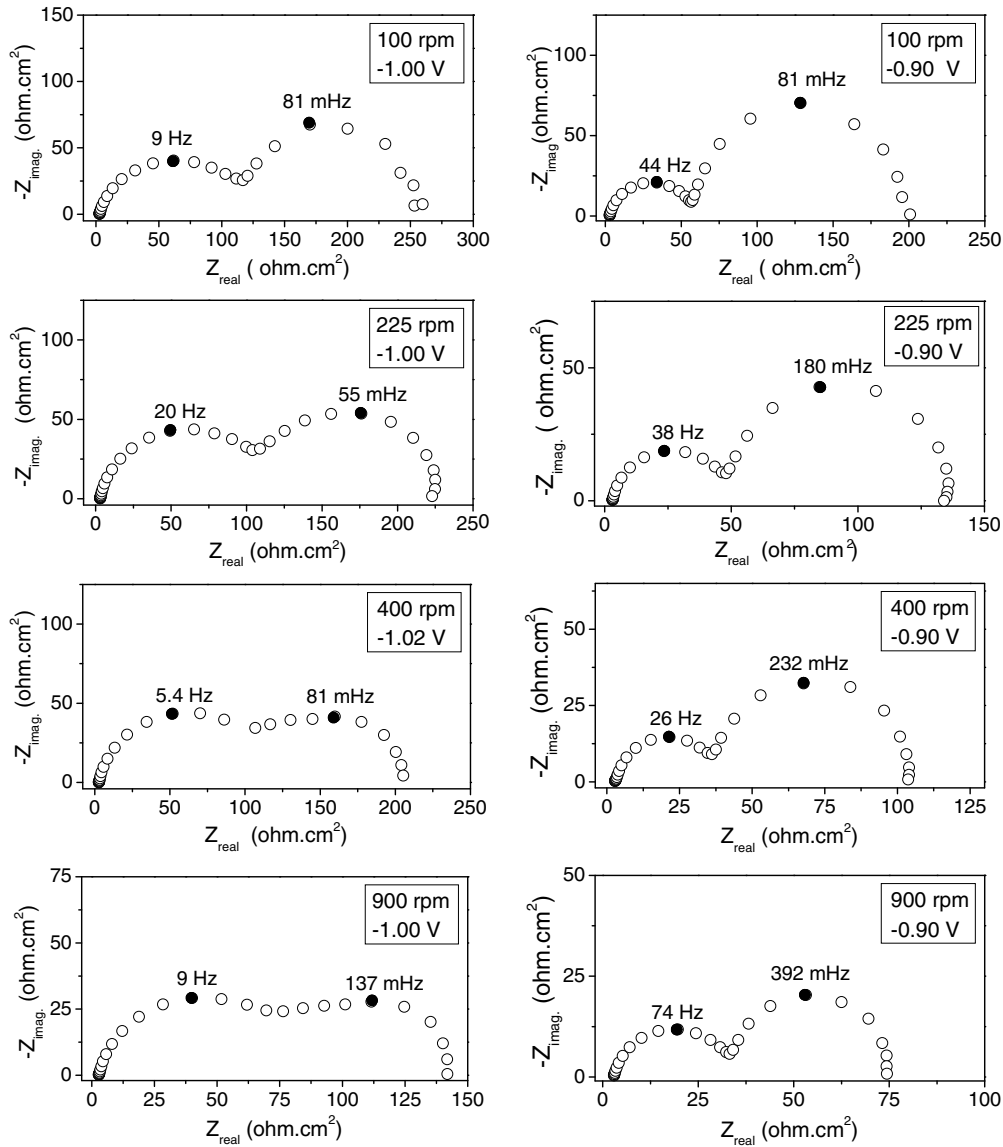
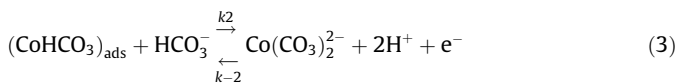
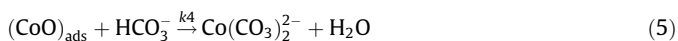
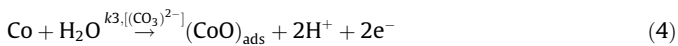


**Fig. 4.** Potentiostatic electrochemical impedance plots of cobalt in 0.75 M  $\text{KHCO}_3$  + 0.05 M  $\text{K}_2\text{CO}_3$  solution at different anodic potential in the active dissolution region and different rotation speed of the electrode.

solution concentrations and under varying hydrodynamic conditions. The presence of two slopes in the steady-state polarisation curves suggested that two different electrochemical paths are taking place during cobalt anodic dissolution, the first path was described as:



The second path was described as:



It appeared that the two electrochemical paths contribute independently to covering the surface with two adsorbed species  $(\text{CoHCO}_3)_{\text{ads}}$  and  $(\text{CoO})_{\text{ads}}$  and it was necessary to introduce a sharing

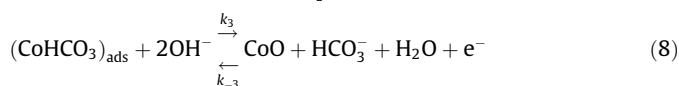
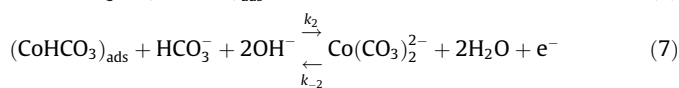
surface parameter ( $\gamma$ ) for the global process. Although the reactions described by Eqs. (2)–(5) explain the steady-state experimental results, it can hardly be used to account for the electrochemical impedance. Indeed, the fluctuation of the sharing surface parameter with the potential is not known and so, can not be used to calculate impedance. On the other hand, the model proposed by S. Real et al. [20] is not considered as an option to explain the present results by following reasons:

- The model does not take into account the presence of  $\text{CoO}$  on the electrode surface, well established in the literature [11–16].
- The model proposes three adsorbed species on the electrode surface and the experimental impedance shows only two loops, one of them related with the double layer.
- Although with three adsorbed species, to avoid three relaxation time constants, the authors have used a very simplified

approach to simulate the experimental results. Indeed, only one adsorbed species, only one theta, was used in the mass and charge balance equations. The two others adsorbed species were completed forgotten.

- The mass transport is considered very simple and classical diffusion impedance was a priori assumed. The model proposed in [20] was not useful to simulate the authors' results. Indeed, the approach used is quite the same presented in the authors' previous paper [19], already analysed in our published work [13].

In the current paper a variation of the previously described reaction [13] is presented, in which it will be no longer necessary to share the surface by  $\gamma$ . We propose that the cobalt anodic dissolution in the first active dissolution region can be explained by the following reactions:



Some remarks can be made regarding the reaction model shown above: cobalt anodic dissolution begins with the formation of the adsorbed species  $(\text{CoHCO}_3)_{\text{ads}}$  as described by reaction (6). Later, anodic dissolution continues through two different paths; the first path involves the formation of the  $\text{Co}(\text{CO}_3)_2^{2-}$  complex by reaction (7). The complex species diffuse from the electrode surface to the bulk solution, as proposed by Davies and Burstein [11]. The second path involves the formation of the CoO oxide from the first adsorbed species (reaction (8)). Metal dissolution also occurs from a fraction of covered cobalt surface by CoO oxide, as described by the autocatalytic reaction (9). In reaction (9) a contribution to total anodic current is achieved without oxide consumption. According to the surface characterisation made with Raman spectroscopy [13] only the CoO oxide is observed on the cobalt surface. The mass transport control observed in steady-state and transient measurements is closely related to the diffusion of the  $\text{Co}(\text{CO}_3)_2^{2-}$  complex.

From the reaction model proposed we can deduce the equations which govern the cobalt anodic dissolution for steady-state and transient conditions in the active metal dissolution region.

#### 4.2. Steady-state condition

Stationary current can be obtained from charge balance made for reactions (6)–(9)

$$\frac{I}{F} = K_1(1 - \theta_1 - \theta_2) + K_2\theta_1 - K_{-2}C_0 + K_3\theta_1 - K_{-3}\theta_2 + 2K_4\theta_2 \quad (10)$$

Mass balance for the same reactions is:

$$\beta_1 \frac{d\theta_1}{dt} = K_1(1 - \theta_1 - \theta_2) - K_2\theta_1 + K_{-2}C_0 - K_3\theta_1 + K_{-3}\theta_2 \quad (11)$$

$$\beta_2 \frac{d\theta_2}{dt} = K_3\theta_1 - K_{-3}\theta_2 \quad (12)$$

where  $\theta_1$  and  $\theta_2$  are the fraction of surface coverage of  $(\text{CoHCO}_3)_{\text{ads}}$  and CoO, respectively.  $\beta_1$  and  $\beta_2$  are the constants which link the concentrations of surface fractions.  $C_0$  is the concentration of  $\text{Co}(\text{CO}_3)_2^{2-}$  on the electrode surface.  $K_i$  is the rate constant for the  $i$ th step defined by:

$$K_i = k_{0,i} \exp\left(\frac{z\alpha F}{RT} \cdot E\right) [\text{HCO}_3^-]_0 \quad (13)$$

The bicarbonate concentration at the electrode surface  $[\text{HCO}_3^-]_0$  is included in the rate constant because, as it was seen in previous work [13], the interfacial pH does not change during the anodic dissolution. Taking into account that the pH is entirely defined by the  $[\text{CO}_3^{2-}]/[\text{HCO}_3^-]$  ratio, suppose that  $[\text{HCO}_3^-]_0$  as a constant is correct. We assumed that elementary steps obey Tafel's law, the transfer coefficient ( $\alpha$ ) has values between 0 and 1 and that coverage by adsorbed species obeys Langmuir's isotherm.

We also assumed that the concentration gradient of the  $\text{Co}(\text{CO}_3)_2^{2-}$  complex is uniformly distributed in a convective diffusion layer with thickness ( $\delta$ ), as shown in Fig. 5. The diffusion of  $\text{Co}(\text{CO}_3)_2^{2-}$  complex with a diffusion coefficient ( $D$ ) follows the classical diffusion law

$$\frac{\partial c(x)}{\partial t} = D \frac{\partial^2 c(x)}{\partial x^2} \quad (14)$$

with the following boundary conditions:

On the electrode surface ( $x = 0$ )

$$D \frac{\partial c(x)}{\partial x} = K_2\theta_1 - K_{-2}C_0 \quad (15)$$

Beyond the diffusion layer ( $x \geq \delta$ ),  $c(x) = 0$

The steady-state is defined by  $\frac{d\theta_1}{dt} = \frac{d\theta_2}{dt} = 0$  and at the electrode surface,

$$\frac{\partial c(x)}{\partial x} = \frac{C_0}{\delta} \quad (16)$$

From Eqs. (15) and (16),

$$C_0 = \frac{K_2}{\frac{D}{\delta} + K_{-2}} \theta_1 \quad (17)$$

and

$$\theta_1 = \frac{K_1 K_{-3} (\frac{D}{\delta} + K_{-2})}{K_1 K_{-3} (\frac{D}{\delta} + K_{-2}) + K_1 K_3 (\frac{D}{\delta} + K_{-2}) + K_{-3} K_2 \frac{D}{\delta}} \quad (18)$$

$$\theta_2 = \frac{K_3}{K_{-3}} \theta_1 \quad (19)$$

The total stationary current is:

$$I_t = F \frac{2K_1 K_2 K_{-3} \frac{D}{\delta} + 2K_1 K_3 K_4 (\frac{D}{\delta} + K_{-2})}{K_1 K_{-3} (\frac{D}{\delta} + K_{-2}) + K_1 K_3 (\frac{D}{\delta} + K_{-2}) + K_{-3} K_2 \frac{D}{\delta}} \quad (20)$$

We look for an anodic current expression that can simulate the experimental polarisation results, similar to the Eq. (1). That is, an expression in which  $\Omega \rightarrow 0$ ,  $I_t = I_0 = f(E)$  and when  $\Omega \rightarrow \infty$ ,  $I_t = I_1 = g(E)$ , where  $I_0$  is a non-diffusion current and  $I_1$  is the current given by

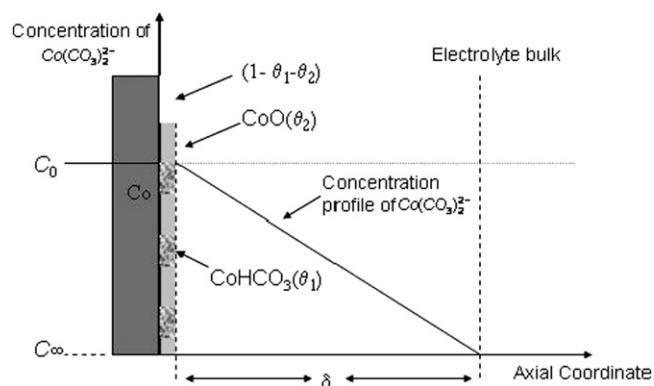


Fig. 5. Schematic representation of the diffusion processes of the  $\text{Co}(\text{CO}_3)_2^{2-}$  complex during the cobalt electrodisolution in 0.75 M  $\text{KHCO}_3$  + 0.05 M  $\text{K}_2\text{CO}_3$  media.

the Koutecky-Levich expression. The right side of Eq. (20) can be rearranged as:

$$I_t = \frac{B\frac{D}{\delta} + C}{M\frac{D}{\delta} + G} \quad (21)$$

where,

$$B = 2F(K_1K_2K_{-3} + K_1K_3K_4) \quad (22)$$

$$C = 2FK_1K_3K_4K_{-2} \quad (23)$$

$$M = K_1K_{-3} + K_1K_3 + K_{-3}K_2 \quad (24)$$

$$G = K_1K_{-2}(K_3 + K_{-3}) \quad (25)$$

Hence, when  $\Omega \rightarrow 0$ ,  $\delta \rightarrow \infty$ , from (21) we have

$$I_t = I_0 = \frac{C}{G} = 2F \frac{K_3K_4}{K_3 + K_{-3}} \quad (26)$$

and when  $\Omega \rightarrow \infty$ ,  $\delta \rightarrow 0$ , we have

$$(I_t - I_0) = \frac{B\frac{D}{\delta} + C}{M\frac{D}{\delta} + G} - \frac{C}{G} \quad (27)$$

Rearranging,

$$(I_t - I_0)^{-1} = \frac{GM}{BG - EC} + \frac{G^2}{(BG - EC)D/\delta} \quad (28)$$

The mass transport coefficient ( $D/\delta$ ) can be written in terms of the Schmidt number ( $Sc$ ) and the rotation speed of the electrode ( $\Omega$ ) as:

$$\frac{D}{\delta} = \frac{D^{1/2}\sqrt{2\pi}}{1.8049Sc^{1/6}} \Omega^{1/2} \quad (29)$$

Then,

$$(I_t - I_0)^{-1} = \frac{GM}{BG - EC} + \frac{G^2}{(BG - EC)K_{MT}} \Omega^{-1/2} \quad (30)$$

where  $K_{MT} = \frac{D^{1/2}\sqrt{2\pi}}{1.8049Sc^{1/6}}$

Eq. (30) can be compared with Eq. (1) and it can be seen that the inverse of the current given by the Koutecky-Levich expression ( $1/I_t$ ) is the right side of Eq. (30), and then we have:

$$\frac{1}{I_t} = \frac{GM}{BG - EC} + \frac{G^2}{(BG - EC)K_{MT}} \Omega^{-1/2} \quad (31)$$

The first term on the right side of Eq. (31) represents the kinetic current under infinite convective mass transport ( $1/I_k$ ), while the second term gives the mass transport contribution ( $1/A$ ) to the total current ( $I_t$ ) recorded at the rotating disk electrode during the anodic dissolution of cobalt.

Consequently, we know that the expression of the total anodic current in terms of the two partial currents  $I_0$  and  $I_1$ , corresponds to the first and second dissolution paths, respectively.

$$I_t = I_0 + I_1 = I_0 + \frac{1}{I_k^{-1} + A^{-1}\Omega^{-1/2}} \quad (32)$$

The similarity of Eq. (32) with Eq. (1) assures that the steady-state results can be very well simulated by Eq. (32), as done in Ref. [13] using the Eq. (1). However, the same kinetic parameter must be used to simulate the impedance results.

#### 4.3. Impedance

From Eqs. (10)–(12) the responses  $\tilde{\theta}_1$ ,  $\tilde{\theta}_2$ ,  $\tilde{C}_0$  and  $\tilde{I}$  to a small amplitude sine wave perturbation  $\tilde{E}$  with variety frequency  $\omega = 2\pi f$ , are

$$\begin{aligned} \beta_2 j\omega \tilde{\theta}_1 = & [b_1 \tilde{K}_1(1 - \theta_1 - \theta_2)\tilde{E} - K_1(\tilde{\theta}_1 - \tilde{\theta}_2) - b_2 \tilde{K}_2 \theta_1 \tilde{E} - K_2 \tilde{\theta}_1 \\ & + b_{-2} \tilde{K}_{-2} C_0 \tilde{E} + K_{-2} \tilde{C}_0 - b_3 \tilde{K}_3 \theta_1 \tilde{E} - K_3 \tilde{\theta}_1 \\ & + b_{-3} \tilde{K}_{-3} \theta_2 \tilde{E} + K_{-3} \tilde{\theta}_2] \end{aligned} \quad (33)$$

$$\beta_2 j\omega \tilde{\theta}_2 = b_3 \tilde{K}_3 \theta_1 \tilde{E} + K_3 \tilde{\theta}_1 - b_{-3} \tilde{K}_{-3} \theta_2 \tilde{E} - K_{-3} \tilde{\theta}_2 \quad (34)$$

$$\begin{aligned} \frac{\tilde{I}}{F} = & [b_1 \tilde{K}_1(1 - \theta_1 - \theta_2)\tilde{E} - K_1(\tilde{\theta}_1 + \tilde{\theta}_2) + b_2 \tilde{K}_2 \theta_1 \tilde{E} + K_2 \tilde{\theta}_1 \\ & - b_{-2} \tilde{K}_{-2} C_0 \tilde{E} - K_{-2} \tilde{C}_0 + b_3 \tilde{K}_3 \theta_1 \tilde{E} + K_3 \tilde{\theta}_1 - b_{-3} \tilde{K}_{-3} \theta_2 \tilde{E} \\ & - K_{-3} \tilde{\theta}_2 + 2b_4 \tilde{K}_4 \theta_2 \tilde{E} + 2K_4 \tilde{\theta}_2] \end{aligned} \quad (35)$$

where  $b_i = \left(\frac{z_i F}{RT}\right)$  for anodic reactions and  $b_{-i} = -\left(\frac{z(1-z_i)F}{RT}\right)$  for cathodic reactions.

From Eq. (15) the diffusion of the  $\text{Co}(\text{CO}_3)_2^{2-}$  complex species follows the expression

$$D \left( \frac{\partial \tilde{C}}{\partial x} \right)_{x=0} = b_2 \tilde{K}_2 \theta_1 \tilde{E} + K_2 \tilde{\theta}_1 - b_{-2} \tilde{K}_{-2} C_0 \tilde{E} - K_{-2} \tilde{C}_0 \quad (36)$$

The equation that describes the mass transport in a transient condition for convective diffusion perpendicular to the electrode surface and at a constant rotation speed of the disk electrode is

$$j\omega \tilde{C} + \bar{V}_x \left( \frac{\partial \tilde{C}}{\partial x} \right) = D \left( \frac{\partial^2 \tilde{C}}{\partial x^2} \right) \quad (37)$$

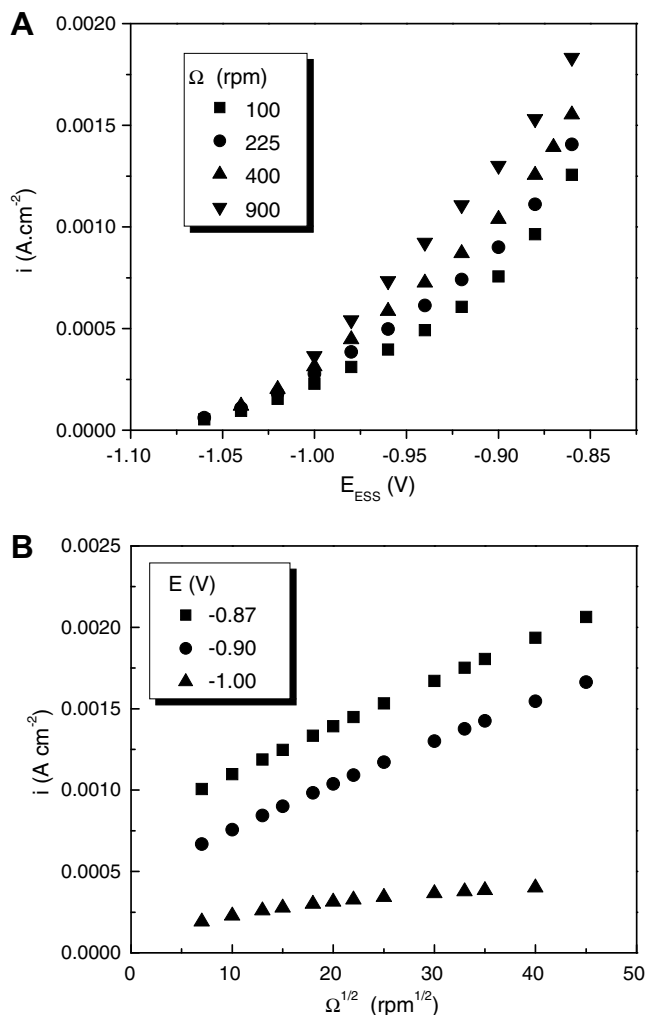


**Fig. 6.** Calculated steady-state polarization curves of cobalt in the active dissolution region at different rotation speeds for the parameter values:  $K_{01} = 0.1019 \times 10^6 \text{ cm s}^{-1}$ ,  $K_{02} = 0.2236 \times 10^7 \text{ cm s}^{-1}$ ,  $K_{0,2} = 0.3461 \times 10^{-5} \text{ cm s}^{-1}$ ,  $K_{03} = 0.4789 \times 10^3 \text{ cm s}^{-1}$ ,  $K_{0,3} = 0.1510 \times 10^{-14} \text{ cm s}^{-1}$ ,  $K_{04} = 0.3308 \times 10^{-1} \text{ cm s}^{-1}$ ,  $\alpha_1 = 0.7930$ ,  $\alpha_2 = 0.7020$ ,  $\alpha_3 = 0.6559$ ,  $\alpha_4 = 0.2349$ ,  $\beta_1 = \beta_2 = 10^{-9} \text{ cm}$ ,  $D = 8 \times 10^{-6} \text{ cm}^2 \text{ s}^{-1}$ , and  $Sc = 1600$ . (A) Current versus voltage plots. (B) Current versus square root of the rotation speed plots.

Following the development made by Tribollet and Newman [21] who obtained the expression for transient gradient concentration of the diffusion species from Eq. (37), we have

$$\left(\frac{\partial \tilde{C}}{\partial x}\right)_{x=0} = \left(\frac{\tilde{C}_0}{\delta}\right)\theta'_{(0)} \quad (38)$$

where  $\theta'_{(0)}$  is the reciprocal of the impedance convective diffusion, also tabulated by Tribollet and Newman in terms of the dimensionless frequency ( $p$ ) and the Schmidt number ( $Sc$ ) [21].

Combining Eqs. (38) and (36) the expression for the transient concentration of the  $\text{Co}(\text{CO}_3)_2^{2-}$  complex is,

$$\tilde{C}_0 = \frac{b_2 \tilde{K}_2 \theta_1 \tilde{E} + K_2 \tilde{\theta}_1 - b_{-2} \tilde{K}_{-2} C_0 \tilde{E}}{K_{-2} - \frac{p}{\delta} (-\theta'_{(0)})} \quad (39)$$

The expression for the faradic electrochemical impedance can be obtained from Eq. (35)

$$\begin{aligned} \frac{1}{Z_F} &= \frac{\tilde{I}}{\tilde{E}} \\ &= \frac{1}{R_t} + F(K_2 + K_3 - K_1) \frac{\tilde{\theta}_1}{\tilde{E}} + F(2K_4 - K_1 - K_{-3}) \frac{\tilde{\theta}_2}{\tilde{E}} - FK_{-2} \\ &\quad \times \frac{\tilde{C}_0}{\tilde{E}} \end{aligned} \quad (40)$$

where  $R_t$  is the charge-transfer resistance, written as

$$R_t = \{F[b_1 K_1 (1 - \theta_1 - \theta_2) + b_2 K_2 \theta_1 - b_{-2} K_{-2} C_0 + b_3 K_3 \theta_1 - b_{-3} K_{-3} \theta_2 + 2b_4 K_4 \theta_2]\}^{-1} \quad (41)$$

And from (33), (34) and (39)

$$\frac{\tilde{\theta}_1}{\tilde{E}} = \frac{H + zM + zN}{G} \quad (42)$$

where

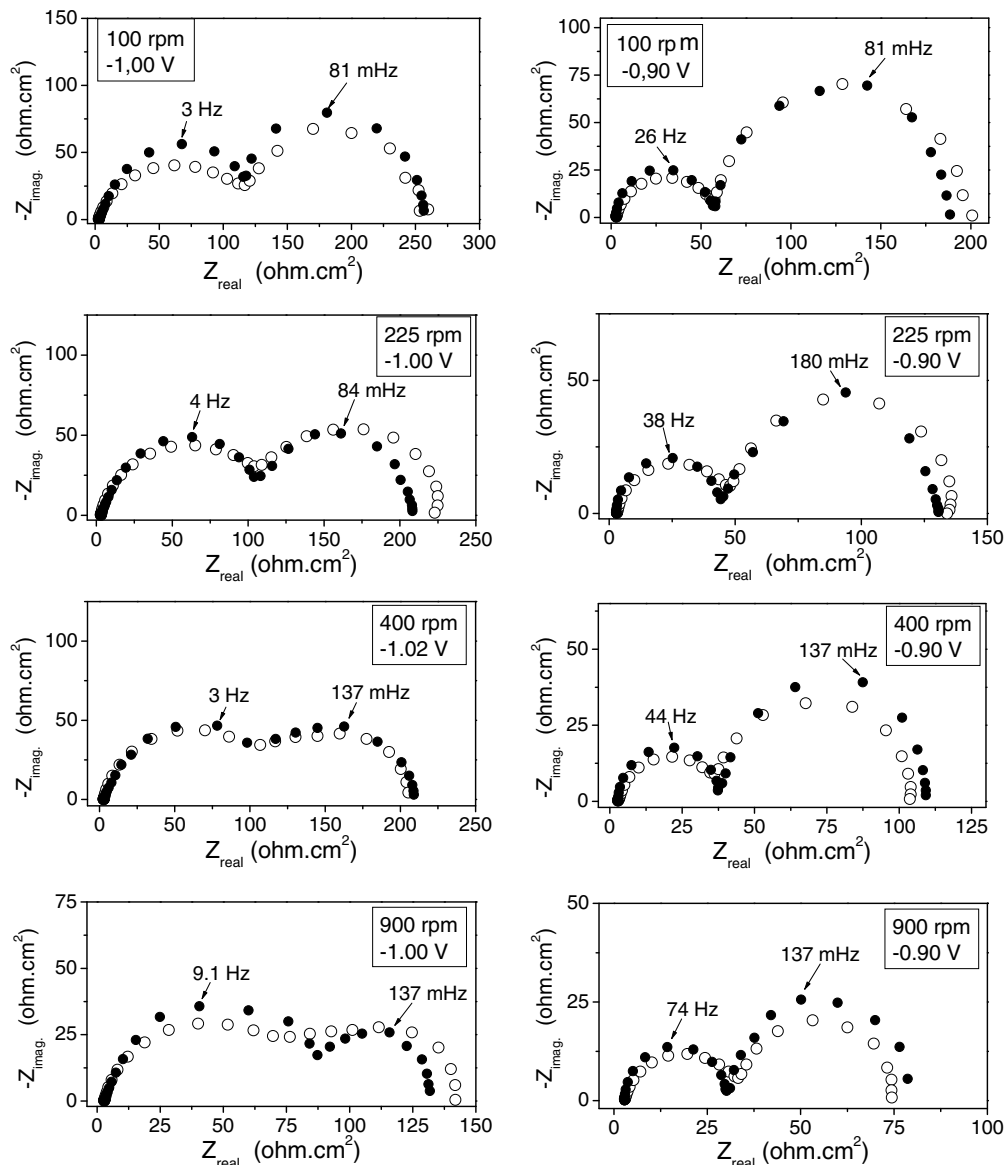


Fig. 7. Calculated electrochemical impedance using the same set of parameter used in the caption of Fig. 6.

$$H = b_1 K_1 (1 - \theta_1 - \theta_2) + b_2 K_2 C_0 + b_3 K_3 \theta_2 - b_2 K_2 \theta_1 - b_3 K_3 \theta_1 \quad (43)$$

$$z_M = \frac{(b_3 K_3 \theta_1 - b_3 K_3 \theta_2)(K_{-3} - K_1)}{\beta_2 j \omega + K_{-3}} \quad (44)$$

$$z_N = \frac{K_{-2}(b_2 K_2 \theta_1 - b_2 K_2 C_0)}{K_{-2} - \left(\frac{\partial}{\partial s}\right)(-\theta'_{(0)})} \quad (45)$$

$$G = \beta_1 j \omega + K_1 + K_2 + K_3 + \frac{K_3(K_1 - K_{-3})}{\beta_2 j \omega + K_{-3}} - \frac{K_2 K_{-2}}{K_{-2} - \left(\frac{\partial}{\partial s}\right)(-\theta'_{(0)})} \quad (46)$$

$$\frac{\tilde{\theta}_2}{\tilde{E}} = \left( \frac{b_3 K_3 \theta_1 - b_3 K_3 \theta_2}{\beta_2 j \omega + K_{-3}} \right) + \left( \frac{K_3}{\beta_2 j \omega + K_{-3}} \right) \frac{\tilde{\theta}_1}{\tilde{E}} \quad (47)$$

$$\frac{\tilde{C}_0}{\tilde{E}} = \left( \frac{b_2 K_2 \theta_1 - b_2 K_2 C_0}{K_{-2} - \left(\frac{\partial}{\partial s}\right)(-\theta'_{(0)})} \right) + \left( \frac{K_2}{K_{-2} - \left(\frac{\partial}{\partial s}\right)(-\theta'_{(0)})} \right) \frac{\tilde{\theta}_1}{\tilde{E}} \quad (48)$$

Then, by substituting  $R_t$ ,  $\frac{\tilde{\theta}_1}{\tilde{E}}$ ,  $\frac{\tilde{\theta}_2}{\tilde{E}}$ ,  $\frac{\tilde{C}_0}{\tilde{E}}$  for their values in Eq. (40) and taking into account the electrolyte resistance ( $R_e$ ) and double layer capacitance ( $C_d$ ), we get the expression for total impedance of the electrochemical process

$$Z_T = R_e + \frac{1}{\frac{1}{Z_f} + j\omega C_d} \quad (49)$$

Simulations of the polarisation and impedance curves were carried out using expressions (32) and (49) respectively. Fig. 6 shows the calculated anodic polarisation curves at different rotation speeds (A), and current versus square root of the rotation speed plots (B), using the kinetic parameters given in the caption of Fig. 6. Fig. 7 shows the calculated impedance plots using the same kinetic parameters for different anodic potentials and rotation speeds. In Table 1 are shown the double layer capacitance values used for simulations at different anodic potentials and rotation speeds of cobalt electrode. High values of  $C_d$  and its changes with potential and rotation speed is an indication that a coupling between the actual  $C_d$  and some adsorb species occurs. This coupling seems to be with  $\theta_1$ , according to admittance analysis, not shown in this paper. The polarisation and impedance curves calculated are similar to the experimental measurements, thus confirming that the reaction model comprised of the reactions (6)–(9) could accurately describe the anodic dissolution of cobalt in the active dissolution region in a carbonate/bicarbonate media. A fitting procedure was not performed because the number of parameters to be fitted is very high. A compromise of the quality of simulation for all results was taken by trial and error. Cobalt electro-dissolution follows two paths, the first path through the formation of the  $\text{Co}(\text{CO}_3)_2^{2-}$  complex and its later diffusion away from the electrode surface, and the second path through the formation of  $\text{CoO}$ . As it can be seen in Fig. 8 (A), each electrochemical path for cobalt dissolution predominates in different regions of the polarisation curves with different participation of the  $I_1$  and  $I_0$  currents to the total anodic process. Those can be also observed in the potential versus  $R_t I$  plot (Fig. 8(B)) in which there is clearly two slopes: one at low and another at high anodic overpotentials. At low anodic overpotentials corresponding to low current densities, metal dissolution occurs principally through the kinetic and mass transport control by the current  $I_1$  and follows the path of reactions (6) and (7), with the formation of the adsorbed  $\theta_1$  ( $\text{CoHCO}_3$ )<sub>ads</sub> and complex species  $\text{Co}(\text{CO}_3)_2^{2-}$ . As it can be seen in Fig. 9, at low anodic overpotentials the fraction of surface coverage of  $\theta_1$  is larger than  $\theta_2$  ( $\text{CoO}$ ). The  $\text{CoO}$  formation from reaction (8) is limited

**Table 1**

Values of electrical double layer capacitance used to impedance simulations for different anodic potentials and rotation speeds

Potential ( $V_{\text{SSE}}$ )	Capacitance ( $\mu\text{F cm}^{-2}$ )			
	100 rpm	225 rpm	400 rpm	900 rpm
-1.02	–	–	240	–
-1.00	60	160	–	160
-0.90	180	200	60	60

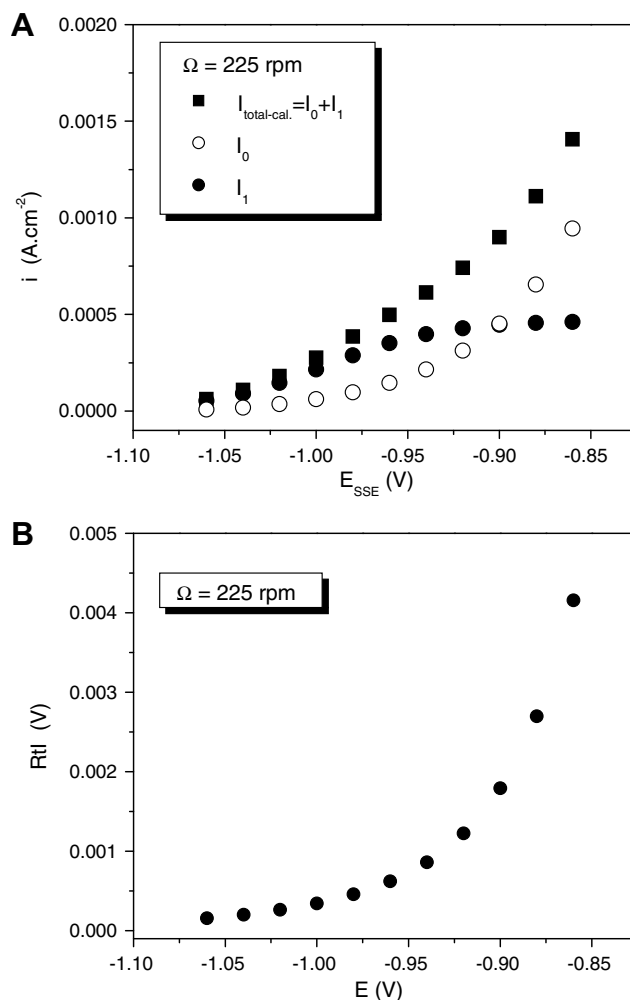


**Fig. 8.** Calculated of total and partial currents at 225 rpm. (A) Anodic total current  $I_t$  and its components  $I_0$  and  $I_1$ . (B) Variation of the product  $R_t I$  versus anodic potential.

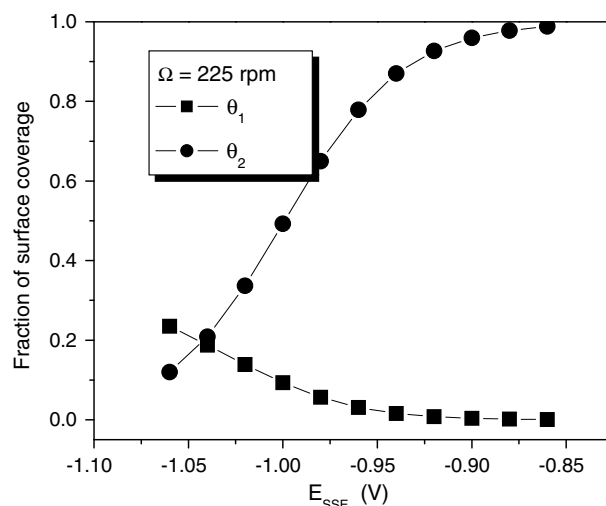


**Fig. 9.** Variation of the fraction coverage surface of  $\theta_1$  ( $\text{CoHCO}_3$ )<sub>ads</sub> and  $\theta_2$  ( $\text{CoO}$ )<sub>ads</sub> versus anodic potential.

because, in this overpotential values,  $K_{-3}$  is larger than  $K_3$ , and the non-diffusion current  $I_0$  is very low. At anodic potential values superior to  $-1.0$  V, the partial current  $I_1$  retains a higher proportion

of the total current. However, because of  $K_3$  exceeds  $K_{-3}$ , the formation of  $\theta_2$  (CoO) is favoured (see Fig. 9). At high anodic overpotentials, the non-diffusion current  $I_0$  forms a higher proportion of the total current, and both  $I_1$  and  $I_0$  contribute to the dissolution of the metal. As it can be seen in Fig. 9, at high anodic overpotentials the formation of adsorbed  $\theta_1$  diminishes and the metal surface is covered principally by  $\theta_2$ . At these anodic potentials both reactions (8) and (9) contribute to the formation of CoO. At high anodic overpotentials, no further increases of the partial current  $I_1$  are observed, mainly due to limited production of  $\theta_1$ . At peak current potential ( $-0.86 V_{SSE}$ ), prior to metal passivation, the contribution of the partial non-diffusion current  $I_0$  to the total anodic current is greater than the contribution of the partial current  $I_1$ . Given these overpotential conditions  $K_3 \gg K_{-3}$  and applying Eq. (26) the expression of the non-diffusion current will be:

$$I_0 = 2FK_4 \quad (50)$$

and the dissolution of metal mainly follows the path of autocatalytic reaction (9). Reaction (8) and (9), will continue to occur, but to a lesser extent. This provides evidence for the non protective characteristic of the CoO film formed on the cobalt surface during the active dissolution of metal.

The impedance diagrams calculated have a similar shape to the experimental diagrams (see Fig. 7). Two capacitive loops were simulated with their respective characteristic frequencies close to the experimental values. The calculated impedance values at zero-frequency limit real part of the impedance, give resistance values close to the polarisation resistance taken from polarisation curves and, as expected, these values decrease with the increase of both anodic polarisation and rotation speed. The relaxations of the second adsorbed species  $\theta_2$  and the diffusion processes have closely linked time constants, all these time constants characterised by the second capacitive loop. The coupling of the time constants makes the linear behaviour of the diffusion process difficult to observe. As it can be seen in Fig. 9 as anodic overpotential increases the surface coverage by  $\theta_2$  became more important, this feature can be follow by the increase of the second capacitive loop at high anodic potentials. Another interesting feature of the second capacitive loop is that its characteristic frequency displays few changes when the anodic potentials and rotation speed are varied, this feature corroborates the existence of an autocatalytic reaction, as in reaction (9), which plays an important role in the dissolution of cobalt at high anodic polarisation.

## 5. Conclusions

A kinetic reaction model is presented to explain cobalt dissolution in a carbonate/bicarbonate media in the potential range be-

tween the open circuit potential and the anodic current peak potential, prior to metal passivation. Two electrodisolution paths were observed during anodic polarisation. We propose that the electrodisolution begins with the formation of intermediate  $(\text{CoHCO}_3)_{\text{ads}}$  on the electrode surface, followed by the simultaneous formation of a  $\text{Co}(\text{CO}_3)_2^{2-}$  complex and the formation of a CoO film. The mass transport phenomenon is characterised by the diffusion of  $\text{Co}(\text{CO}_3)_2^{2-}$  away from the electrode surface. At low anodic polarisation, the formation of  $(\text{CoHCO}_3)_{\text{ads}}$  is greater than the formation of CoO film, but when the anodic potential increases, formation of the CoO film is favoured due to an autocatalytic reaction. Experimental polarisation and impedance measurements were simultaneously simulated by mathematic expressions derivate from the kinetic reaction model.

## Acknowledgements

The authors are grateful for the support given by the Colombian agencies: Colciencias, and the New Materials Excellence Centre (CENM), and Brazilian agencies: CAPES and CNPq. The authors thank B. Tribollet (CNRS-PARIS) for the fruitful discussion of the present results.

## References

- [1] Elke Rahm, Dagmar Kunzmann, Helke Döring and Rudolf Holze, *Microchim. Acta* 156 (2006) 141.
- [2] E. Gomez, E. Pellicer, E. Valles, *Electrochem. Commun.* 7 (2005) 275.
- [3] W.A. Badawy, F.M. Al-Kharafi, J.R. Al-Ajmi, *J. Appl. Electrochem.* 30 (2000) 693–704.
- [4] C.M. Chun, J.D. Mumford, T.A. Ramanarayanan, *J. Electrochem. Soc.* 150 (2003) B76.
- [5] R.D. Cowling, A.C. Riddiford, *Electrochim. Acta* 14 (1969) 981.
- [6] W.K. Behl, J.E. Toni, *J. Electroanal. Chem.* 31 (1971) 63.
- [7] T.R. Jayaraman, V.K. Venkatesan, H.V.K. Udupa, *Electrochim. Acta* 20 (1975) 209.
- [8] G.W. Simmons, E. Kellerman, H. Leidheiser Jr., *J. Electrochem. Soc.* 123 (1976) 1276.
- [9] N. Sato, T. Ohtsuka, *J. Electrochem. Soc.* 125 (1978) 1735.
- [10] C.A. Melendrese, S. Xu, *J. Electrochem. Soc.* 131 (1963) 2239.
- [11] D.H. Davies, G.T. Burstein, *Corros. Sci.* 20 (1980) 973.
- [12] G.T. Burstein, D.H. Davies, *Corros. Sci.* 20 (1980) 989.
- [13] J.A. Calderón, O.R. Mattos, O.E. Barcia, S.I. Córdoba de Torresi, J.E. Pereira da Silva, *Electrochim. Acta* 47 (2002) 4531.
- [14] C.A. Gervasi, S.R. Biaggio, J.R. Vilche, A.J. Arvia, *Corros. Sci.* 29 (1989) 427.
- [15] C.A. Gervasi, S.R. Biaggio, J.R. Vilche, A.J. Arvia, *Electrochim. Acta* 36 (1991) 2147.
- [16] C.A. Gervasi, J.R. Vilche, P.E. Alvarez, *Electrochim. Acta* 41 (1996) 455.
- [17] D. Gallant, S. Simard, *Corros. Sci.* 47 (2005) 1810.
- [18] D. Gallant, M. Pézolet, A. Jacques, S. Simard, *Corros. Sci.* 48 (2006) 2547.
- [19] S.G. Real, *J. Brazil. Chem. Soc.* 8 (1997) 153.
- [20] S.G. Real, S.B. Ribotta, A.J. Arvia, *Corros. Sci.* 50 (2008) 463.
- [21] B. Tribollet, J. Newman, *J. Electrochem. Soc.* 130 (1983) 2016.